The Effect of Forward-Facing Steps on Stationary Crossflow Instability Growth and Breakdown

Jenna L. Eppink*

NASA Langley Research Center, Hampton, VA 23681

The effect of a forward-facing step on stationary crossflow transition was studied using standard stereo particle image velocimetry (PIV) and time-resolved PIV. Step heights ranging from 53 to 71% of the boundary-layer thickness were studied in detail. The steps above a critical step height of approximately 60% of the boundary-layer thickness had a significant impact on the stationary crossflow growth downstream of the step. For the critical cases, the stationary crossflow amplitude grew suddenly downstream of the step, decayed for a short region, then grew again. The adverse pressure gradient upstream of the step resulted in a region of crossflow reversal. A secondary set of vortices, rotating in the opposite direction to the primary vortices, developed underneath the uplifted primary vortices. The wall-normal velocity disturbance (V') created by these secondary vortices impacted the step, and is believed to feed into the strong vortex that developed downstream of the step. A large but very short negative crossflow region formed for a short region downstream of the step due to a sharp inboard curvature of the streamlines near the wall. For the larger step height cases, a crossflow-reversal region formed just downstream of the strong negative crossflow region. This crossflow reversal region is believed to play an important role in the growth of the stationary crossflow vortices downstream of the step, and may be a good indication of the critical forward-facing step height.

Nomenclature

c	chord length
N	N-factor
Re'	Unit Reynolds number
Tu	turbulence intensity
U	streamwise velocity component
u'	fluctuating components of velocity
U', V'	steady disturbance velocity
u'_{rms}	temporal root mean square of u'
U'_{rms}, V'_{rms}	spanwise root mean square of steady disturbance velocity, U', V'
U_e	boundary layer edge velocity
U_∞	freestream velocity
$U_\perp$	velocity component normal to the step
V	wall-normal velocity component
$W_\parallel$	velocity component parallel to the step
W_{cf}	velocity component normal to the local inviscid streamline
x	streamwise direction
x_c	direction normal to the leading edge
x_s	streamwise location of step
x_{sh}	number of step heights downstream of step
y	wall-normal direction

*Research Aerospace Engineer, Flow Physics and Control Branch, M.S. 170, AIAA Member

z	spanwise direction (parallel to the leading edge)
Symbols	
ΔN	shift in N-factor due to the excrescence
δ	boundary-layer thickness, location where U=0.99U_e
λ_z	spanwise wavelength

I. Introduction

THERE exists a constant push in the aerospace sciences toward improving the fuel efficiency of commercial transport aircraft. One possible approach to this problem, which has been long been studied, is the implementation of laminar-flow surfaces. This approach is only recently beginning to make its way onto commercial transport aircraft due to the technical challenges associated with maintaining laminar flow on operational aircraft. While some companies are already implementing natural laminar flow on their transport aircraft surfaces, such as Boeing's 737 MAX Winglet and the 787 engine nacelles,[1] the wings, which provide a much larger surface area and therefore much more potential for drag reduction, remain largely untapped. One of the major remaining challenges is the potential for any small surface protuberance or excrescence to prematurely trip the flow, resulting in a significant or even complete loss of any drag reduction benefit. These excrescences could be the result of insect contamination during operation, or the result of necessary manufacturing defects, such as steps, gaps, or bolts. In order to have confidence that a significant amount of laminar flow benefit will be maintained, we need to be able to establish achievable (i.e., not too conservative) manufacturing tolerances. To do this, we need to be able to accurately predict critical roughness heights.

In order to develop better prediction models for acceptable roughness levels, we need to understand the mechanisms that cause transition when the surface imperfections are present. The transition mechanisms will likely vary depending on the type of surface imperfection. One approach to predicting the effect of 2D excrescences on transition is the use of a semi-empirical method known as the ΔN method.[2–4] An empirical equation is used to estimate an expected increment in N-factor (i.e., the ΔN) across the 2D excrescence. These studies have focused on 2D (unswept) geometries, but the effect of 2D steps on swept-wing transition has gained more interest recently. This work has generally been limited to observing the behavior of the transition front as the step height is increased,[5,6] but more recently, researchers have begun to study the flow in more detail. These studies are important because of the complexity of the transition process over excrescences. The understanding is that the boundary layer will be modified by the excrescence, which will impact the instabilities in the flow, causing either an increase or decrease in growth (or no change). How the modified mean flow will impact the instabilities, what (if any) new types of instabilities are introduced by the step, and how these new instabilities interact to lead to transition are all problems that need to be addressed in order to better understand and predict transition.

Duncan et al.[7] performed hotwire measurements downstream of forward- and backward-facing steps to determine the effect of the steps on stationary crossflow instabilities. They found that the steps caused an increase in N-factor for the stationary crossflow. The forward-facing step (FFS) caused a larger growth of the stationary crossflow than the backward-facing step (BFS). Tufts et al.[8] performed computations to study the interaction between stationary crossflow instabilities and a two-dimensional step excrescence. The forward-facing step, above a critical height, was found to substantially increase the growth of the stationary crossflow mode. They suggest that the mechanism for this increased growth involves a constructive interaction between the incoming stationary crossflow vortex and the helical flow region just downstream of the step. Thus, they propose that if one can predict the height of the center of the incoming crossflow vortex from the baseline state, then this should be close to the critical step height, since this is the height at which the crossflow vortex and helical flow region would begin to interact constructively.

Eppink[9] experimentally studied the effect of forward-facing steps on stationary crossflow growth by performing stereo particle image velocimetry (SPIV) measurements. The steps above the critical height caused a large increase in the growth of the stationary crossflow instability just downstream of the step, resulting in earlier transition. The results agreed qualitatively with the computational results of Tufts et al.[8] The critical step height predicted using the approach suggested by Tufts et al.[8] was about 15% higher than the actual critical step height found in the experiment. Additionally, it was found that increasing the initial stationary crossflow amplitude resulted in premature transition for a previously subcritical step height. The goal of the current work is to better understand the mechanism that causes the increased amplitude of the stationary crossflow mode near the step. To this end, we perform both standard and time-resolved PIV

(TRPIV) measurements to obtain mean data upstream and downstream of the step. The time-resolved data downstream of the step also provide interesting results related to the breakdown mechanism that occurs.

II. Experimental Setup

The experiment was performed in the 2-Foot by 3-Foot Low Speed Boundary-Layer Channel at the NASA Langley Research Center. The tunnel is a closed circuit facility with a 0.61-m high by 0.91-m wide by 6.1-m long test section. The tunnel can reach speeds up to 45 m/s ($Re' = 2.87$ x 10^6/m) in the test section. Freestream turbulence intensity levels, $Tu = \frac{1}{U_\infty}\sqrt{\frac{1}{3}(u'^2 + v'^2 + w'^2)}$, were measured using a crosswire in an empty test section to be less than 0.06% for the entire speed range of the tunnel, and less than 0.05% for the test speed of 26.5 m/s. This value represents the total energy across the spectrum, high-pass filtered at 0.25 Hz. Thus, this tunnel can be considered a low-disturbance facility for purposes of conducting transition experiments.[10]

The 0.0127-m thick flat plate model consists of a 0.41-m long leading edge piece, swept at 30°, and a larger downstream piece (see Fig. 1). The model is 0.91 m wide (thus, spanning the width of the test section) and 2.54 m long on the longest edge. The downstream or leading edge pieces can be adjusted relative to each other using precision shims to create either forward-facing or backward-facing 2D steps of different heights, parallel with the leading edge. The leading edge piece was polished to a surface finish of 0.2 μm, and the larger downstream plate had a surface finish of 0.4 μm. A leading-edge contour was designed for the bottom side of the plate in order to make the suction-peak less severe, and therefore, avoid separation, which could potentially cause unsteadiness in the attachment line.

A 3D pressure body along the ceiling was designed to induce a streamwise pressure gradient, which, along with the sweep, causes stationary crossflow growth. A second purpose of the ceiling liner was to simulate infinite swept-wing flow within a midspan measurement region of width 0.3 meters. This was achieved by designing the liner such that the C_p contours were parallel with the leading edge within the measurement region. The ceiling liner was fabricated out of a hard foam using a computer-controlled milling machine.

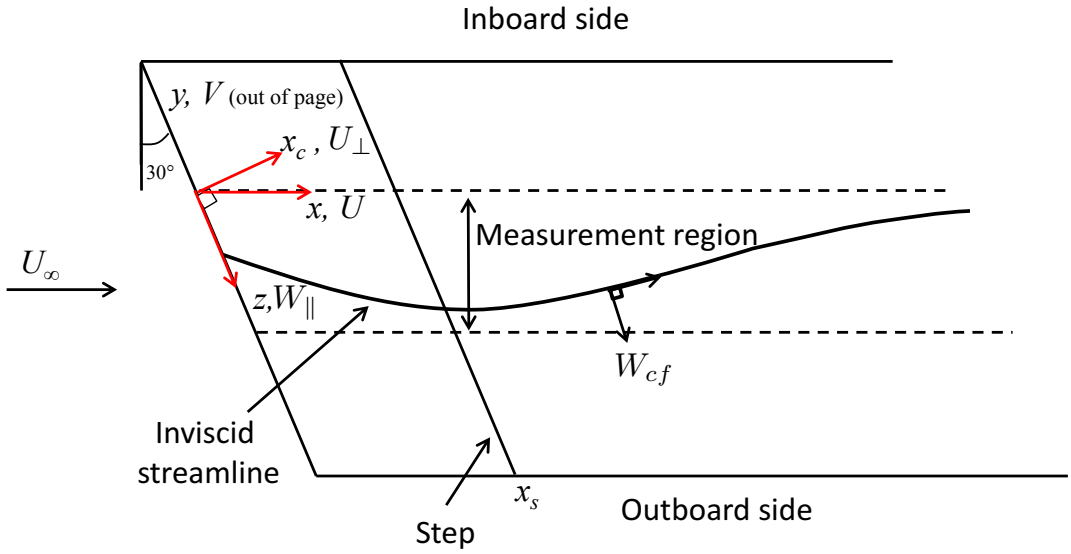

Figure 1: Model sketch and coordinate system.

Due to the complexity of the flow field, it is sometimes necessary to examine different components of velocity. The coordinate systems used are defined in Fig. 1. The streamwise direction is denoted by x, whereas x_c denotes the normal-chord direction. The velocity components in these directions are denoted by U and $U_\perp$, respectively. The direction parallel to the leading edge is denoted by z, with the velocity

component in that direction denoted by $W_{\parallel}$. Finally, the velocity in the direction normal to the local inviscid streamline is denoted by W_{cf}. The mean disturbance quantities, which are acquired by subtracting the spanwise-averaged profile from each individual profile at a given x location, are denoted using capital letters with an apostrophe, such as U'. The time-fluctuating components are denoted using lower-case letters with an apostrophe, i.e., u'.

All measurements were performed at a freestream velocity of 26.5 m/s ($Re' = 1.69$ x 10^6/m). The current experiment utilized two leading-edge roughness configurations consisting of discrete roughness elements (DREs) with a diameter of 4.4 mm. The DREs were applied with a spanwise spacing, λ_z, of 11 mm and were approximately 20 μm thick. The spacing of the DREs (11 mm) corresponds to the most amplified stationary crossflow wavelength calculated for the baseline case with no step. Most of the cases presented were acquired with a single layer of DREs applied near the leading edge. One case was acquired in which four layers of DREs were stacked to increase the height of the DREs to approximately 80 μm. This case is referred to as the 1.4 mm FFS case with 4 layers of DREs. For more details of the experiment setup, refer to Eppink.[11]

A high-speed double-pulsed Nd:YLF laser provided the laser sheet for the PIV measurements (see Fig. 2). The laser sheet was set up parallel with the leading edge and the forward-facing step. Two pairs of cameras were setup separately, the downstream pair using the high-speed cameras for TRPIV, and the upstream pair using standard 10 Hz PIV cameras. Most of the data were initially acquired using the downstream pair of cameras, but this setup did not allow measurements near the surface upstream of the step. Thus, the second pair of cameras were set up to allow acquisition upstream of the step without needing to move the downstream pair of cameras.

The two high-speed 4-megapixel cameras that were used to acquire the TRPIV measurements were placed downstream of the step. One was placed on the outboard side of the test section at approximately 30° to the laser sheet, and the second camera was placed on the inboard side (in backward scattering) at an angle of approximately 45° to the laser sheet (Fig. 2). To achieve the desired field of view and resolution, 300 mm lenses were utilized, resulting in a total possible measurement area of approximately 60 mm x 30 mm. For the majority of the measurements, the area of interest was reduced to approximately 60 mm x 8 mm to obtain an acquisition rate of 2 kHz. This area allowed acquisition of approximately five wavelengths of the stationary crossflow instability in a single frame, while still acquiring approximately 30 points (using 75% overlap and 24x24 pixel interrogation size) inside the boundary layer. For the mean flow measurements, data were acquired starting near the step and moving downstream at approximately 1 mm increments. Five hundred image pairs were acquired at each location. For selected locations, measurements were acquired at a faster rate of 8 kHz, for which the area of interest was necessarily reduced further to approximately 15 mm x 5 mm, allowing acquisition of just over one wavelength of the stationary crossflow instability. For these measurements, 10,000 image pairs were acquired.

A pair of two-megapixel cameras were placed upstream of the step on the inboard side of the test section and were used to acquire data at 10 Hz. Using 300 mm lenses for these cameras, the resulting area of interest was approximately 30 mm x 30 mm, allowing acquisition of almost three wavelengths of the stationary crossflow instability. For this arrangement, 500 image pairs were acquired at each location. All cameras and the laser were mounted on the same traversing system, which allowed measurements at multiple locations with relative ease. An oil-based fog machine generated the seeding with a particle size of approximately 1 μm, which was introduced downstream of the test section.

III. Results and Discussion

A. Overview of Cases Studied

Measurements were performed for 5 step heights ranging from 1.27 mm to 1.7 mm with a single layer of DREs applied to the leading edge. These step heights correspond to a range of 53 to 71% of the local unperturbed boundary-layer thickness (δ) at the step location. An additional case was studied for the 1.4 mm step case, which included additional layers of DREs to increase the initial stationary crossflow amplitude. The critical step height was found to be approximately 1.6 mm, meaning that at or above this step height, transition moved upstream relative to the no-step case. The 1.52 mm case was found to be subcritical since transition did not move upstream, however, the stationary crossflow amplitudes near the step were significantly impacted. They eventually decayed back to the baseline amplitudes,[9] so the transition front did not move. The 1.4 mm case resulted in slight increased growth of the stationary crossflow near

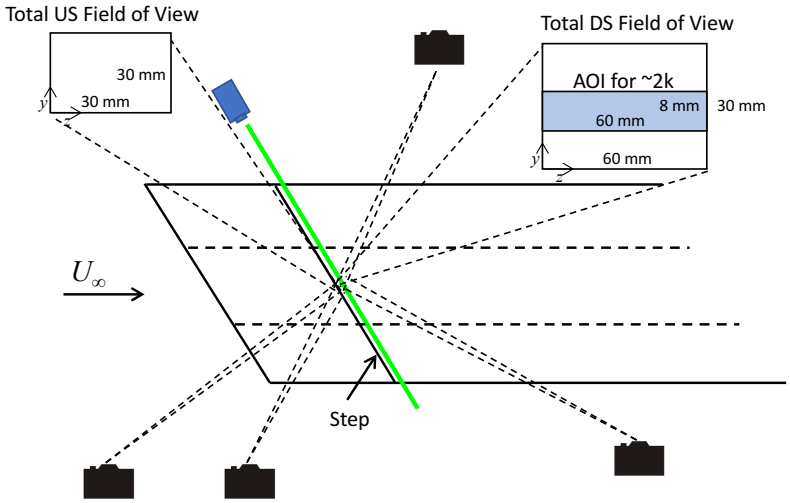

Figure 2: Top view of PIV setup.

the step, but again did not result in premature transition. However, the 1.4 mm step height with the increased stationary crossflow amplitude resulted in transition shortly downstream of the step, showing that the incoming stationary crossflow amplitude plays a role in the interaction. The transition locations relative to the step location for each step height are plotted in Fig. 3.

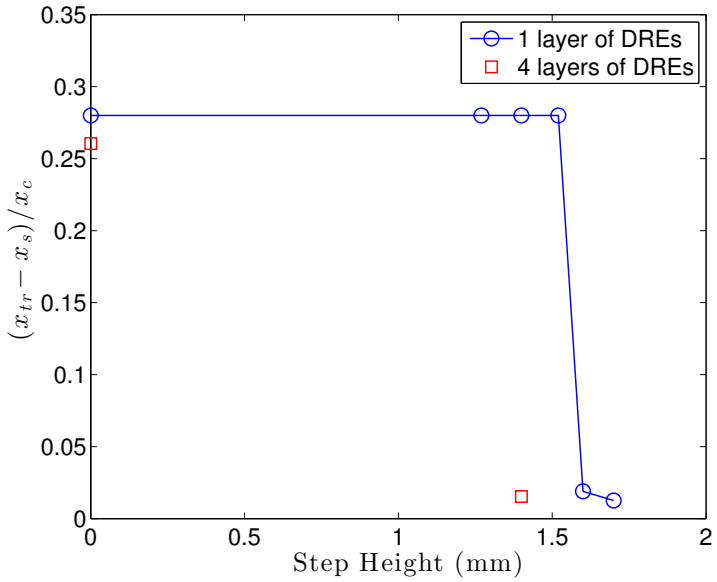

Figure 3: Transition location vs. step height.

B. Effect of Steps on Mean Flow

It is beneficial to start by examining the behavior of the mean flow near the step. Results for three velocity components are shown in Fig. 4 for the 1.4 mm FFS case upstream and shortly downstream of the step. The velocity components normal and parallel to the step are plotted ($U_\perp$ and $W_\parallel$, respectively), along with the wall-normal component (V). Near the step there is a short region of strong positive wall-normal velocity, which reaches amplitudes of over 10% of the freestream $U_\perp$ component. There is a noticeable kink that

occurs right at the step ($x - x_s \approx 0$) in the $U_\perp$ velocity (Fig. 4a), but not in the $W_\parallel$ velocity (Fig. 4c). Just upstream of this location, the boundary layer is gradually thickening, so the wall-normal velocity gradient is gradually decreasing, but suddenly the boundary layer becomes thinner and the $U_\perp$ wall-normal velocity gradient increases for a short distance before beginning to decrease again. Similar behavior was observed for all step heights that were studied. This behavior of the $U_\perp$ velocity can be explained simply through continuity. Consider the continuity equation:

$$\frac{\partial U_\perp}{\partial x_c} + \frac{\partial V}{\partial y} + \frac{\partial W_\parallel}{\partial z} = 0 \tag{1}$$

Since the $W_\parallel$ component is not expected to change in the z direction due to the infinite swept wing flow, we can assume $\frac{\partial W_\parallel}{\partial z} \approx 0$. Therefore, $\frac{\partial U_\perp}{\partial x_c} \approx -\frac{\partial V}{\partial y}$. Figure 5a shows individual V profiles for several locations upstream and downstream of the step. There are two things to note from this figure. First, there is a positive peak in the V component inside the boundary layer, meaning that $\partial V/\partial y$ changes sign. Second, this peak location first moves toward the wall, until just downstream of the step, where it moves abruptly away from the wall. This change in direction of the peak corresponds exactly to the location of the abrupt change in the $U_\perp$ profiles. Consider a point in the boundary layer in between y=2 and y=2.5 mm in Fig. 5a. Initially (at $x - x_s$=-2.3 mm), $\partial V/\partial y$ is positive, because this location is below the peak location. However, moving downstream ($x - x_s$=0.5 mm), the peak location moves below y=2 mm, so $\partial V/\partial y$ becomes negative, meaning that $\partial U_\perp/\partial x_c$ now must become positive. But then at the next measurement station, $x - x_s$=1.5 mm, the V peak lifts up again above this point, so $\partial V/\partial y$ becomes positive again, and thus $\partial U_\perp/\partial x_c$ suddenly becomes negative. The $U_\perp$ and $W_\parallel$ components at $y = 2.25$ mm are plotted vs. x in Fig. 5b to further illustrate this point. Initially, $U_\perp$ and $W_\parallel$ are decreasing at about the same rate, until $x - x_s$=0.5 mm, at which point $W_\parallel$ continues to decrease, but $U_\perp$ suddenly increases for one point before decreasing again.

The maximum V-velocity was found to increase with increasing step height, which is expected. However, the location of the maximum of the V-velocity in the boundary layer did not change relative to the step height. Thus, the wall-normal shear of the V-component ($\partial V/\partial y$) near the wall and downstream of the step increases with increasing step height, meaning that this effect should be increased as the step height is increased.

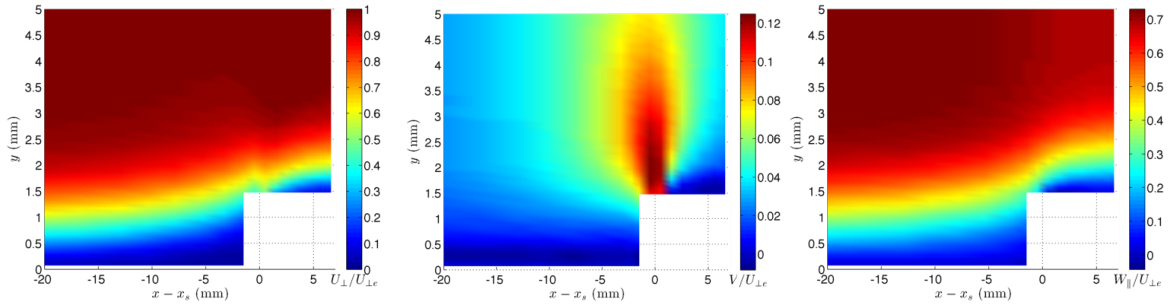

(a) $U_\perp$ **(b)** V **(c)** $W_\parallel$

Figure 4: Spanwise-averaged profiles upstream and downstream of the step for the 1.4 mm step case.

This sudden change in the $U_\perp$ is important because it results in a sudden inboard curvature of the streamlines near the wall, which results in very large negative crossflow. Crossflow occurs when the streamlines near the wall become more curved than the inviscid streamlines, resulting in flow normal to the inviscid streamline direction within the boundary layer. In a typical swept wing flow, the streamline curvature near the wall is higher than the inviscid streamline curvature simply because the velocity near the wall is lower, while the spanwise pressure gradient is essentially unchanged across the height of the boundary layer. However, in this case, the increased streamline curvature near the wall may be due to a combined effect of the inviscid streamline curvature as well as the strong V component near the step, which causes an abrupt change in $U_\perp$.

Figure 6 includes plots of both the inviscid streamline and near-wall streamline angles for each step height. The angles shown here (Ψ) are relative to the normal chord (x_c) direction. These angles were

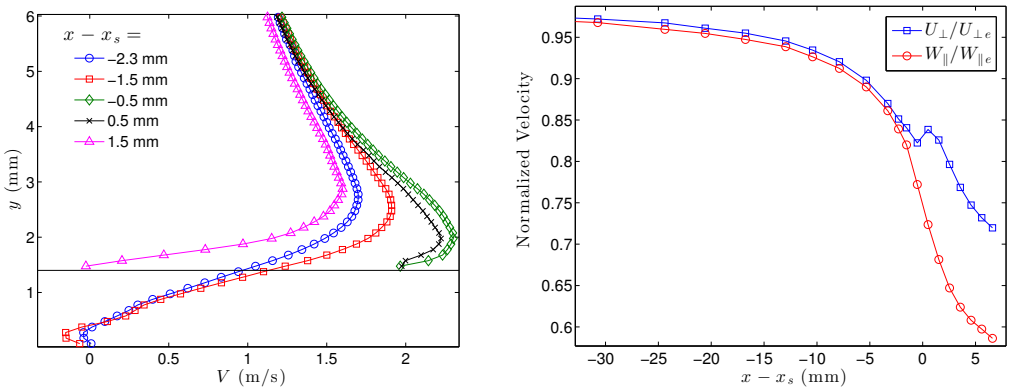

(a) Spanwise-averaged V profiles from several $x - x_s$ locations.

(b) Spanwise-averaged velocity at y=2.25 mm

Figure 5: Results for the 1.4 mm FFS illustrating the V profiles and the abrupt change in $U_\perp$ near the step.

computed using the spanwise-averaged mean velocity components, $U_\perp$ and $W_\parallel$, at each streamwise location. The near-wall streamlines were computed at y=0.1 mm relative to the step height. Upstream of the step, the inviscid streamlines (Fig. 6a) start to turn slightly toward the inboard side, until about 10 mm downstream of the step, where they turn back outboard.

The near-wall streamlines (Fig. 6b) undergo more drastic changes in direction compared to the inviscid streamlines (included on the same plot for comparison). Starting just downstream of the step, the near-wall streamlines turn inboard sharply. The location of this sharp decrease in streamline angle corresponds to the same point ($x - x_s$=0.5 mm) at which the abrupt change occurs in the $U_\perp$ velocity. At approximately 4 mm downstream of the step, the angle of the streamlines for the smallest step height (1.27 mm) begins to increase gradually until becoming nearly constant at approximately 31 degrees. The larger step heights, however, undergo a sharp increase in streamline angle starting at approximately 4 mm downstream of the step. This increase continues, and the angles reach values larger than the inviscid streamline angles, starting between 5 and 10 mm downstream of the step. When the near-wall streamline angle reaches larger values than the inviscid streamline angle, this indicates that the flow is experiencing crossflow reversal near the wall. There is a clear effect of step height on the maximum angle of the near-wall streamlines downstream of the crossflow-reversal region. These angles increase with increasing step height and peak at $x - x_s \approx 15$ mm before gradually decreasing back to the downstream value of approximately 31 degrees.

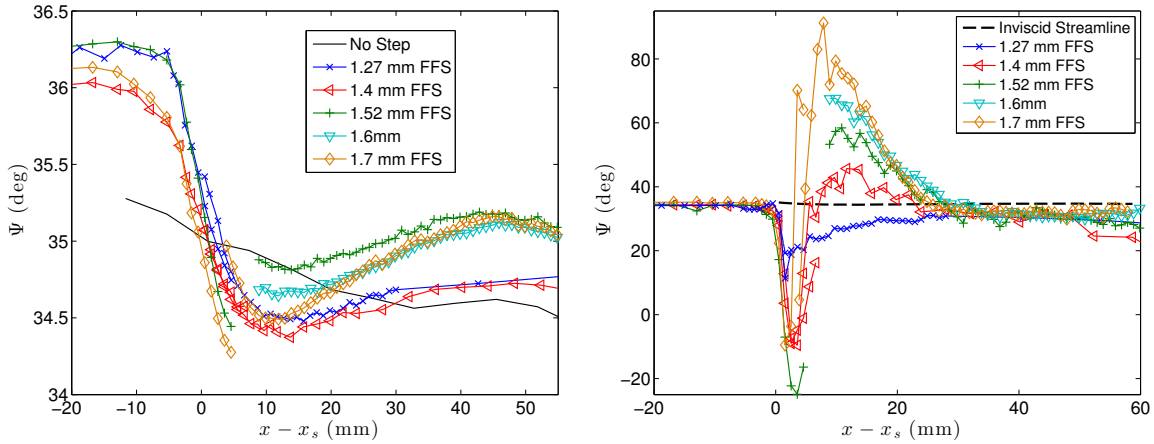

(a) Freestream (inviscid) streamlines **(b) Near-wall (y=0.1 mm) streamlines**

Figure 6: Freestream (inviscid) and near-wall streamline angles vs x for all cases studied.

The crossflow velocity component (W_{cf}) is plotted for three different step heights in Fig. 7. Additionally, individual profiles are included in Fig. 8b for the 1.7 mm FFS case. These results illustrate the effect that the streamline curvature has on the crossflow component inside the boundary layer. The abrupt inboard curvature of the streamlines near the wall just downstream of the step results in the large negative crossflow component that can be seen for all three cases. Near the wall, this strong negative crossflow region lasts for only a few millimeters. In the case of the largest step height, 1.7 mm, there is a positive crossflow velocity component that occurs near the wall starting at approximately 3 mm downstream of the step and extending until approximately 20 mm. The positive crossflow region coincides with the region shown in Fig. 6b in which the near-wall streamline angles became larger than the inviscid streamline angle. There is also a region upstream of the step for all three cases in which a positive crossflow component was measured, starting approximately 20 mm upstream of the step. This crossflow reversal region becomes stronger as the step height is increased.

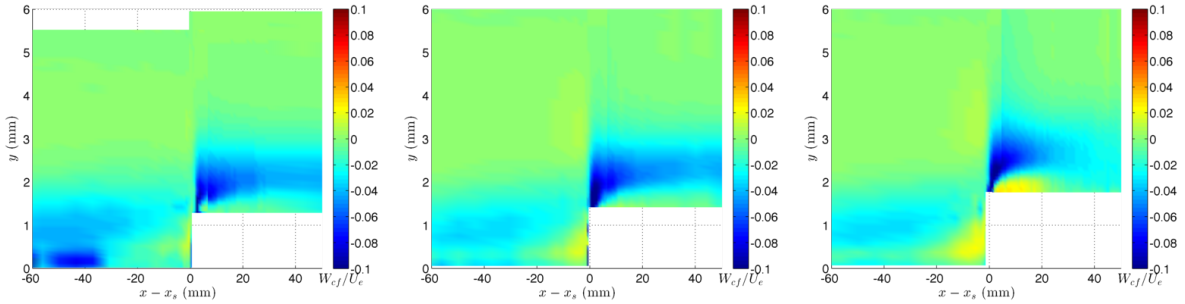

(a) 1.27 mm FFS **(b) 1.4 mm FFS** **(c) 1.7 mm FFS**

Figure 7: Spanwise-averaged crossflow velocity (W_{cf}) profiles upstream and downstream of the step for three different step heights.

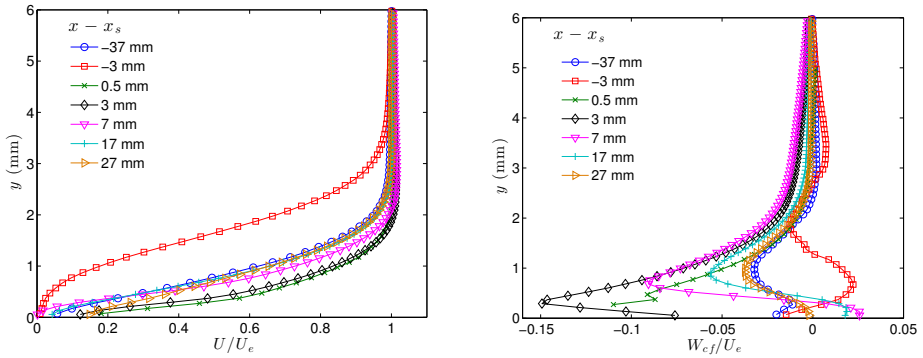

(a) U-profiles **(b) W_{cf}-profiles**

Figure 8: Selected profiles upstream and downstream of the step for the 1.7 mm FFS case.

In the undisturbed case, the crossflow direction inside the boundary layer is typically from outboard to inboard (i.e., negative in this case) due to the imposed favorable pressure gradient, as can be seen far upstream of the step. However, crossflow reversal (i.e., a change in sign of the crossflow component) can occur when the streamline curvature direction changes due to a change in the sign of the streamwise pressure gradient. Tufts et al.[8] noted that upstream of a swept forward-facing step the flow undergoes a region of adverse pressure gradient, followed by a short region of favorable pressure gradient at the step, and then another region of adverse pressure gradient downstream of the step. Thus, the adverse pressure gradients that are encountered upstream and downstream of the step likely contribute to the crossflow reversal that occurs upstream of the step for all cases, and downstream of the step for the larger step heights. The rotation direction of the stationary crossflow vortices is determined by the direction of the crossflow velocity in the boundary layer since this determines the sign of the vorticity at the inflection point. Therefore, crossflow reversal (i.e., a change in sign of the W_{cf} velocity) can result in the amplification of stationary crossflow vortices rotating in the opposite direction to the initial primary vortices.

Several individual U and W_{cf} profiles are plotted in Fig. 8 for the 1.7 mm FFS case to further illuminate the effect that the step has on the mean flow. One profile is included far upstream of the step to show the original state of the boundary layer before the step has any influence. Just upstream of the step, the U profile is lifted up. It is expected that there is a small amount of recirculation at this point, but no negative U velocity was measured, likely because the amplitude is very small. Just downstream of the step, the boundary layer thickness is immediately reduced to about half of what it was upstream of the step. It is also significantly thinner (by approximately 30%) at this point than the unperturbed boundary layer far upstream of the step. This could have an important effect on the stability of the flow downstream of the step. A thinner boundary layer means that smaller wavelength disturbances will be more highly amplified. This could explain the effect mentioned by Tufts et al.,[8] that smaller wavelength disturbances become affected at smaller step heights. By about 17 mm downstream of the step, the U profile appears to have relaxed back to the profile from far upstream of the step.

The crossflow profile shown in Fig. 8b far upstream of the step illustrates the normal negative crossflow direction (i.e., outboard to inboard). Just upstream of the step, the negative peak has been lifted up significantly, and a positive peak is evident near the wall, indicating crossflow reversal. Downstream of the step, at 0.5 and 3 mm, a strong negative crossflow component occurs abruptly. This strong negative peak begins to decay, and a positive crossflow component is evident very near the wall in the profiles starting 7 mm downstream of the step. This positive peak near the wall decays and by 27 mm downstream of the step, the profile appears to have relaxed back to the unperturbed case. Several of these profiles do not return to a velocity of 0 at the wall, which should be the case. It is believed that this discrepancy is due to the large gradients at the wall and the limited resolution of the measurement technique near the surface.

The thinner boundary layer downstream of the step results in a substantial and sudden increase in the wall-normal shear of the U velocity component ($\partial U/\partial y$). Fig. 9 shows profiles of $\partial U/\partial y$ for three of the step heights studied. Starting immediately downstream of the step, there is a sudden increase in $\partial U/\partial y$ near the wall, but this value begins to decrease immediately downstream. The behavior of $\partial U/\partial y$ near the step is important for interpreting the stationary crossflow results and will be discussed further in the next section.

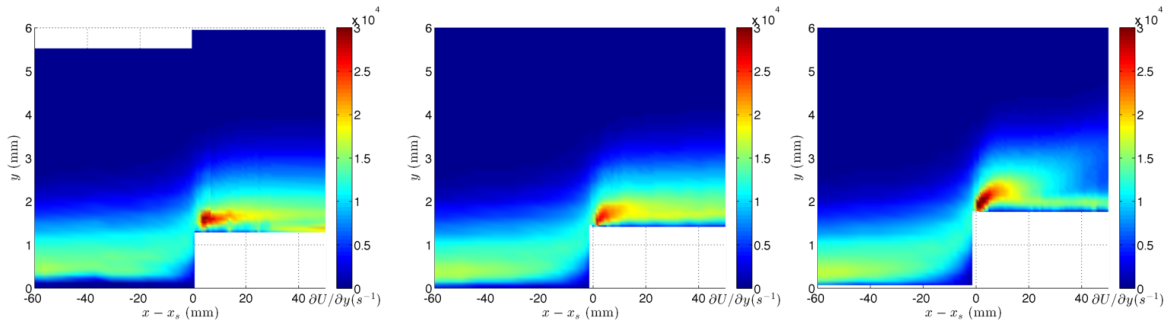

(a) 1.27 mm FFS **(b) 1.4 mm FFS** **(c) 1.7 mm FFS**

Figure 9: Spanwise-averaged dU/dy profiles upstream and downstream of the step for three different step heights.

Several individual profiles of the wall-normal crossflow velocity gradient ($\partial W_{cf}/\partial y$) are plotted in Fig. 10 to show the effect that the step has on the location of the inflection point of the crossflow profile. An inflection point is indicated by a positive or negative peak in the $\partial W_{cf}/\partial y$ profile. The location of the inflection point is important because that is typically the y-location where the instabilities develop. A positive peak in $\partial W_{cf}/\partial y$ indicates the inflection point that exists for the negative crossflow component of flow, and the reverse is also true. Far upstream of the step, the primary inflection point is positive, and occurs at $y \approx 1.5$ mm. As the step is approached, this positive peak lifts up, and a negative peak occurs underneath, at approximately y=1 mm. This negative peak corresponds to the development of the positive crossflow upstream of the step. Immediately downstream of the step, the positive peak $\partial W_{cf}/\partial y$ increases, and this inflection point moves close to the wall, and then slowly lifts up downstream of the step as the amplitude decays. Another inflection point develops underneath this one, with a large negative value of $\partial W_{cf}/\partial y$. Again, this negative peak in $\partial W_{cf}/\partial y$ indicates the development of the crossflow reversal region (i.e., positive crossflow) downstream of the step. The two inflection points are located very close spatially in y, and indicate the propensity for two sets of crossflow vortices to develop, rotating in opposite directions. This will be explored further in the next section.

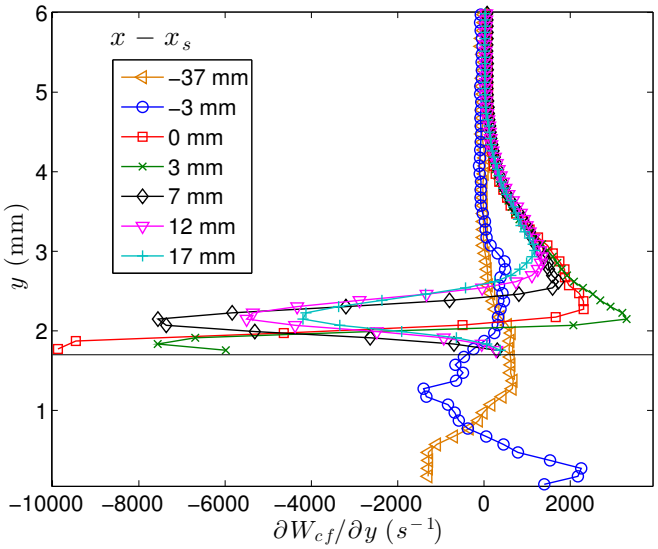

Figure 10: Selected $\partial W_{cf}/\partial y$ profiles upstream and downstream of the step for the 1.7 mm FFS case.

C. Effect of Steps on Stationary Crossflow

Figure 11 shows the U-perturbation profiles for most of the step heights studied, both upstream and downstream of the step. The U-perturbation profiles are calculated from the RMS of the steady disturbance velocity (U') across the span (integrated across a wavelength range of 5 to 20 mm). The 1.6 mm FFS height case is omitted from this figure since no upstream measurements were performed for this case. Note the different color scales in these figures. As seen in previous measurements and computations,[8,9] for the critical step heights, there is a large amount of growth of the U'_{rms} disturbance near the wall just downstream of the step. Upstream of the step, the primary incoming disturbance gets lifted up. For the larger step heights ($\geq$ 1.52 mm), this disturbance forms an upper lobe that eventually decays and disappears, while the near-wall peak starts out very large near the step, then decays, and then begins to grow again around 20 mm downstream of the step. For the two smaller step heights, the upper lobe seems to persist and dominate downstream, while the lower peak decays and disappears.

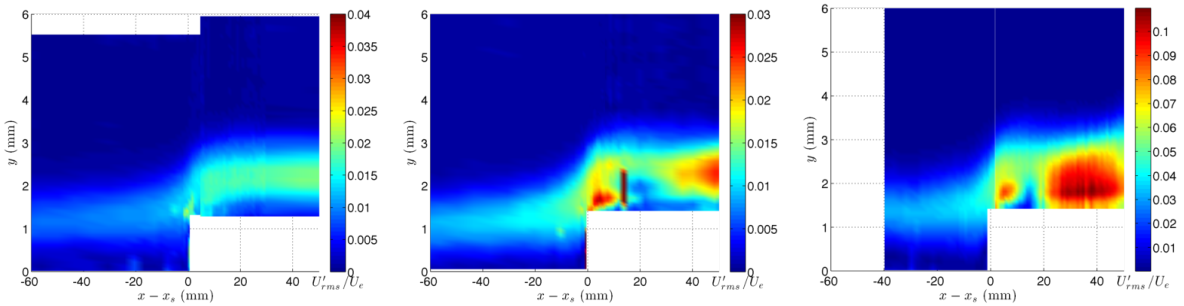

(a) 1.27 mm FFS **(b) 1.4 mm FFS** **(c) 1.4 mm FFS, 4 layers of DREs**

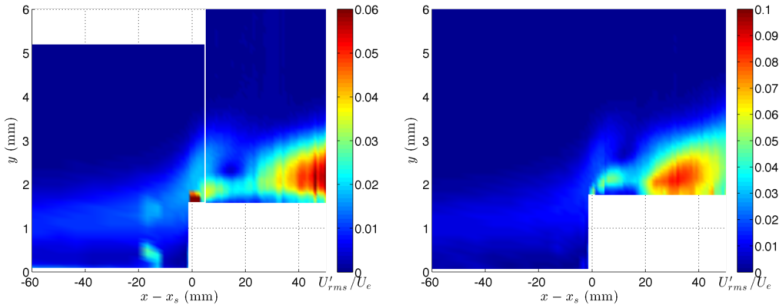

(d) 1.5 mm FFS **(e) 1.7 mm FFS**

Figure 11: U'-perturbation profiles upstream and downstream of the step. Note the different color scales.

The V-perturbation profiles are computed similarly to the U-perturbation profiles, but using the V' component. These profiles are shown in Fig. 12. The V-velocity is about two orders of magnitude smaller than U, except for the region close to the step. Thus, these velocities are much more difficult to measure accurately using PIV, and there is a lot more noise visible in these plots, particularly for the smaller step heights where the V'_{rms} amplitudes remain small. The results for the 1.27 mm and 1.4 mm FFS cases are difficult to interpret for this reason. However, the 1.4 mm FFS case with 4 layers of DREs, as well as the 1.52 mm and 1.7 mm FFS cases, result in significantly larger amplitudes of V'_{rms}. The 1.4 mm step height with four layers of DREs (Fig. 12c) causes significant growth of V'_{rms} both near the surface and away from the surface near the step. Similar to the lift-up of U'_{rms} seen in Fig. 11c, in this case we can see the incoming V'_{rms} peak being lifted up as it approaches the step. Additionally, there is a second peak in the V'_{rms} profile that occurs closer to the surface upstream of the step. Though not visible in Fig. 12c due to the color scale, the secondary peak begins to grow shortly downstream of the location where the positive crossflow velocity component near the wall first appears (see Fig. 7). Since the direction of rotation of the stationary crossflow vortices is determined by the direction of the crossflow in the boundary layer, these near-wall stationary crossflow vortices are rotating in the opposite direction of the primary crossflow (upper set of vortices) due

to this positive crossflow component. Notice that it is the lower set of vortices that directly impacts the step. This lower V'_{rms} peak experiences a significant amount of growth just downstream of the step before decaying for a short distance, until approximately 5 mm downstream of the step, where it begins to grow again. Starting at $x - x_s \approx 15$ mm, the V'_{rms} profile begins to broaden significantly. Meanwhile, the upper V'_{rms} peak experiences a smaller but still significant amount of growth near the step before it decays for a short distance but then appears to merge with the lower peak before the broadening of the profile starting at $x - x_s$=15 mm.

Somewhat different behavior is observed for the two larger step heights (Figs. 12d-12e). In these cases, there is a large amount of growth of V'_{rms} near the wall starting at the step, but there is no clear region of decay. The amplitude grows fairly continuously for both cases. Additionally, the upper lobe near the step gets lifted up (similar to the 1.4 mm FFS case), but instead of merging back in farther downstream, this lobe disappears. The V'_{rms} profile begins to broaden significantly starting close to $x - x_s$=10 mm, similar to the 1.4 mm FFS with 4 layers of DREs.

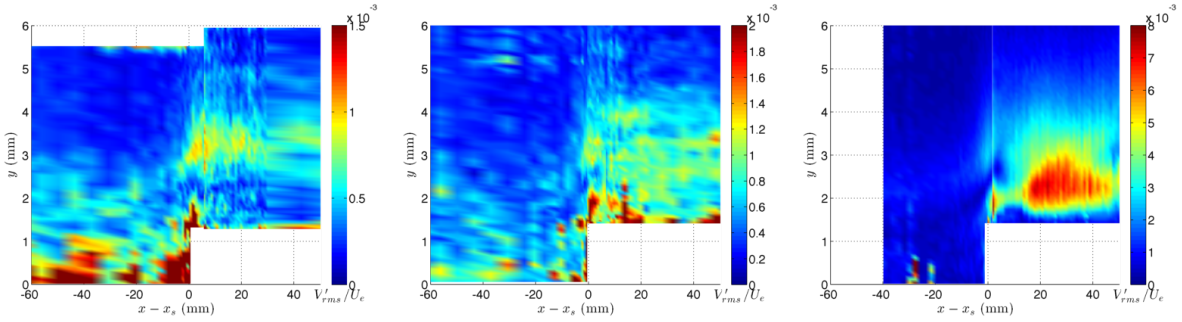

(a) 1.27 mm FFS **(b) 1.4 mm FFS** **(c) 1.4 mm FFS, 4 layers of DREs**

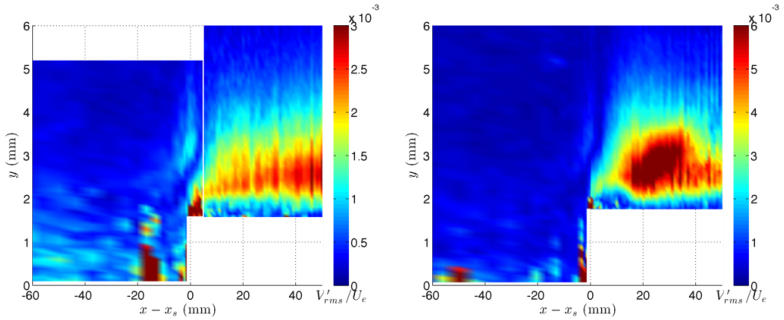

(d) 1.5 mm FFS **(e) 1.7 mm FFS**

Figure 12: V'-perturbation profiles upstream and downstream of the step. Note the different color scales.

Several individual profiles taken from Figs. 11e and 12e are shown in Fig. 13 for the 1.7 mm FFS case to help clarify some of the previous discussion. Just downstream of the step, the U'_{rms} amplitude increases near the wall. A little farther downstream ($x - x_s$=12 and 17 mm), the amplitude decreases and two clear lobes are present in the profiles. After 17 mm, the two peaks merge into one and the amplitude near the wall grows very large. The V'_{rms} profile upstream of the step exhibits two peaks (Fig. 12e). The upper peak corresponds to the incoming primary stationary crossflow vortices, and the lower peak corresponds to the secondary set of vortices that form due to the crossflow reversal upstream of the step. Downstream of the step ($x - x_s$=3mm), there is still a remnant of the upper peak that quickly decays. A large peak forms near the wall immediately downstream of the step. This peak grows and lifts up off the wall as the flow progresses downstream. After $x - x_s$=7 mm, the V'_{rms} profile becomes very broad and increases significantly in amplitude.

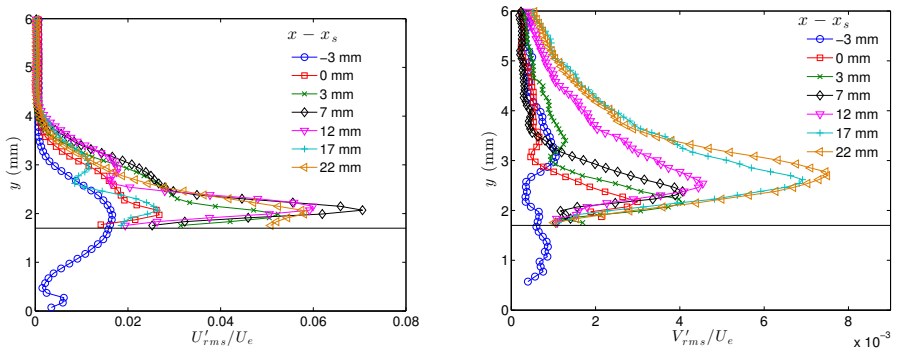

(a) U'_{rms} profiles **(b) V'_{rms} profiles**

Figure 13: Selected crossflow disturbance profiles for the 1.7 mm FFS case

Some lift-up of the primary incoming stationary crossflow vortices is noticeable from the U'_{rms} and V'_{rms} contour plots shown in Figs. 11-12. To illustrate this more clearly, several U-perturbation profiles upstream of the step are plotted. These profiles are shown at four locations upstream of the step in Fig. 14 for two step heights: 1.4 mm and 1.7 mm. As they approach the step, the profiles begin to lift up by a significant amount. In the 1.4 mm step case, the total amount of lift up that occurs from 60 mm upstream of the step to 2 mm upstream of the step is approximately 0.8 mm. In the 1.7 mm step case, the lift up is slightly higher, at approximately 0.9 mm. There is also a slight increase in amplitude as the step height is increased, which is particularly visible at the location closest to the step ($x - x_s$=-2 mm).

This lift up shows that the incoming stationary crossflow vortex does not directly impact the step, indicating that the approach of using the center of the crossflow vortex from the undisturbed flow condition as a prediction of the critical step height probably does not have a physical basis. As mentioned previously, there is a second peak in the V'_{rms} profile that occurs underneath the primary peak, indicating the existence of a secondary set of vortices. This secondary peak is the one that impacts the step. These secondary vortices are rotating in the opposite direction of the primary vortices, so they would not be expected to interact constructively with the helical flow region downstream of the step.

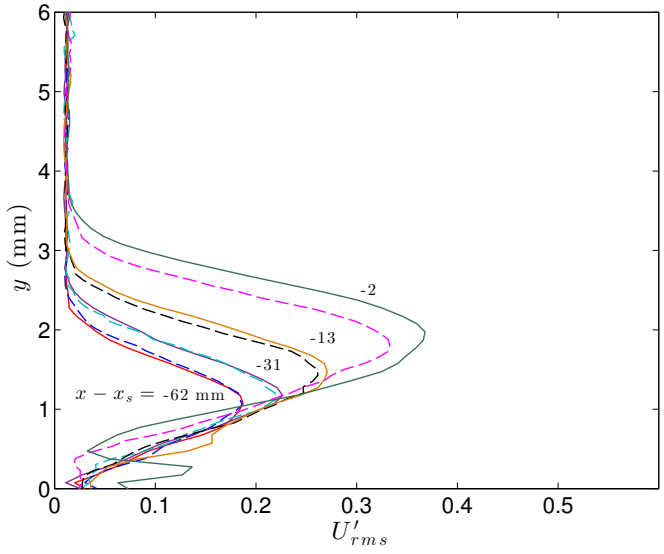

Figure 14: Stationary crossflow U-perturbation profiles upstream of the step. Solid lines are for 1.7 mm FFS, dashed lines are 1.4 mm FFS.

The peak amplitudes of the U'_{rms} and V'_{rms} profiles are plotted vs. x in Fig. 15. The results are normalized

by the most upstream amplitude of the respective no-step cases. As illustrated in the contour plots (Figs. 11 and 12), the U'_{rms} profiles for step heights greater than or equal to 1.4 mm resulted in enhanced growth of the stationary disturbance shortly downstream of the step, followed by a short region of decay, and later subsequent growth. Interestingly, the growth rates of both 1.4 mm step cases agree very well near the step, until 20 mm downstream of the step. At this point, the amplitude grows rapidly for the larger amplitude case (4 layers of DREs), but there is not much of a second growth for the lower amplitude case. This behavior suggests that the mechanism behind this second region of growth may be nonlinear, while the initial growth and decay is probably a linear effect.

The growth of the V'_{rms} disturbance amplitude (Fig. 15b) is similar to that of the U'_{rms} disturbance amplitude. There is a sharp growth in amplitude starting just upstream of the step, but the region of decay just downstream of the step is much shorter and the amount of amplitude decay not very significant, particularly for the larger step heights ($\geq$ 1.52 mm). This difference between the U'_{rms} and V'_{rms} growth is also noticeable in the contour plots shown in Figs. 11-12, as well as the profiles plotted in Fig. 13.

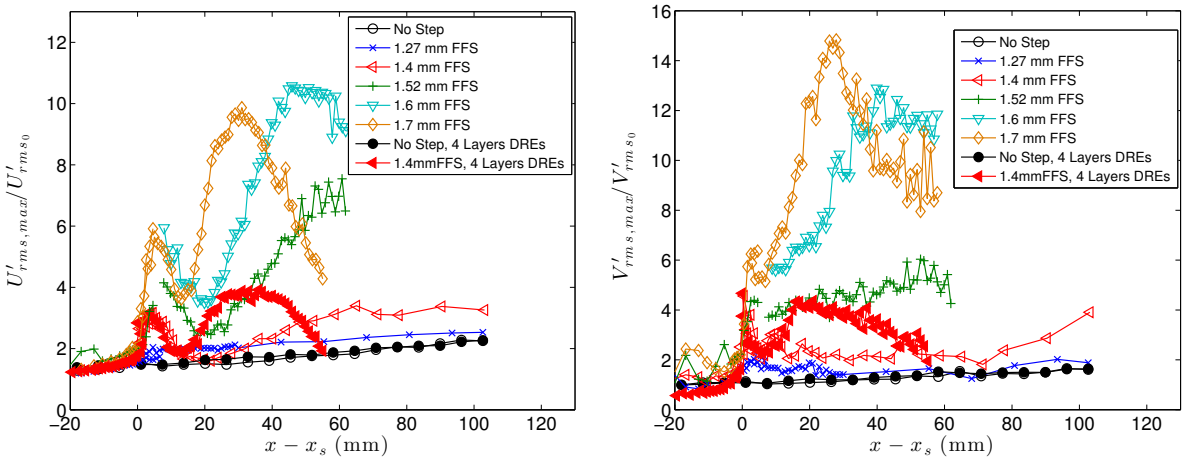

(a) U'_{rms} **(b)** V'_{rms}

Figure 15: Peak amplitude of U' and V'-perturbation profiles upstream and downstream of the step.

The large negative crossflow component near the step (see Fig. 7) caused by the sharp decrease in streamline angle near the wall correlates well with the first sharp peak and decay in the growth of the V'_{rms} disturbance (Fig. 15b). Shortly thereafter, the V'_{rms} amplitude begins to grow again for most of the step cases (excluding 1.27 mm and 1.4 mm with one layer of DREs). This second growth appears to correlate with the beginning of the crossflow reversal region downstream of the step.

When interpreting the V'_{rms} and U'_{rms} results, it is important to keep in mind the complexity of the flow field. In a typical swept wing boundary layer, the growth of the V'_{rms} and U'_{rms} amplitude should directly coincide. The V'_{rms} amplitude is essentially a measurement of the vortex strength, while the U'_{rms} amplitude is a measurement of the effect of the stationary crossflow vortices on the mean flow. When a step is introduced into the flow, the results become much more difficult to decipher. There are several notable differences in the mean flow that could affect the interpretation of these results. The most important is the effect of the step on $\partial U/\partial y$, as shown in Fig. 9. Another thing to keep in mind is the fact that the mean flow is changing drastically over a short distance. This means that U' needs some time to respond to the sudden changes in V'.

The difference in the growth patterns of U'_{rms} and V'_{rms} downstream of the step can partially be explained by the fact that there is a region of high wall-normal shear near the surface beginning at the step (Fig 9). The distortion of the U profiles (and hence, the growth of U'_{rms}) occurs through the convection of the fluid due to the action of the vortices (consider the terms $V\frac{\partial U}{\partial y}$ and $W\frac{\partial U}{\partial z}$ from the momentum equation). Thus, the U'_{rms} amplitude is dependent not only on the amplitude of the stationary crossflow vortices (i.e., V'_{rms}), but also on the amplitude of the wall-normal shear ($\partial U/\partial y$). Since the amplitude of $\partial U/\partial y$ is large near the step but decreases downstream, U'_{rms} can be expected to follow a similar pattern, even if V'_{rms} does not, as

long as the effect of the decaying $\partial U/\partial y$ overpowers the effect of the growth of V'_{rms}.

We have established that the crossflow reversal upstream of the step results in a set of vortices underneath the primary vortices, which are rotating in the opposite direction. The question remains, what role, if any, do these vortices play in the transition scenario downstream of the step. To illustrate what occurs immediately upstream of the step, results are shown from two different $y-z$ planes just upstream and downstream of the step for the 1.4 mm FFS case with four layers of DREs in Fig. 16. This case with increased stationary crossflow amplitude is used to illustrate this point because the V' disturbance becomes much clearer when the amplitude is larger. To acquire the streamlines in these plots, first the wave angle of the stationary crossflow vortex is determined by finding the angle at which the crossflow component goes to 0 at the inflection point. We then use the spanwise-averaged profile for this component, along with the V' values, to obtain the streamlines.

There are two sets of vortices present upstream of the step, as expected. The upper vortex is centered at $y \approx 2.6$ mm, and the lower one at $y \approx 1.5$ mm. The upper set of vortices is rotating in the clockwise direction, while the lower set is rotating in the counter-clockwise direction. The spatial phase of the upper and lower sets of V' disturbances (Fig. 16a) are offset by almost 180°, meaning that the two sets of vortices are located almost directly above and below each other. In Fig. 16d, the same streamlines are plotted along with color contours of U'. We can see the effect of the upper set of vortices (which are the primary incoming vortices) on the U' disturbances, the peak of which is located below the center of the upper vortex. It is typically the case that the peak of U'_{rms} occurs below the peak of V'_{rms}. However, in this case, the vortex, and thus V'_{rms}, has been lifted up significantly above the U' disturbance. Notice that where V' is negative, the vortex is pulling high momentum fluid down, so U' in that similar location is positive, and the inverse is also true. At this point, the lower set of vortices do not appear to have had a very large impact on the U' disturbance.

Figures 16b and 16e show similar results for the first plane acquired downstream of the step. There is one set of vortices that is located very close to the surface and is rotating clockwise. This is expected due to the strong negative crossflow component that occurs right at the step. Two sets of V' disturbances are still noticeable downstream of the step, at y$\approx$ 1.6 and 3 mm. However, the upper set has been lifted up above the region where the crossflow vortices are active. This occurs due to the sudden change in the location of the inflection point downstream of the step. Now it is the lower set of V' disturbances that is influencing the vortices. Thus, the lower set of vortices coming into the step, which form due to the crossflow reversal upstream of the step, creates the V' disturbance that exists near the wall downstream of the step. When the inflection point suddenly moves closer to the surface downstream of the step, a vortex forms close to the wall and feeds off the existing V' disturbance. The upper set of vortices, which corresponds to the initial stationary crossflow mode that existed far upstream of the step, gets lifted up and does not appear to influence what happens near the step.

Notice in Fig. 16e and 16f that the U' contours that persist downstream of the step no longer align with the action of the vortices. In other words, where the vortex is pulling down high momentum fluid, the U' velocity is not positive. Thus, the vortices that form directly downstream of the step are actually counteracting the existing meanflow modulation. This is another feature of this flow field that can make the interpretation of the U'_{rms} disturbances very challenging. At the last station shown here (Figs. 16c and 16f), the V' contours have shifted slightly from their upstream locations. The upper and lower sets of V' disturbances appear to be merging. The U' contours from the upstream location are lifting up, and a larger amplitude peak is growing near the wall and offset to the right from the original set. The vortices also lift up and shift slightly to the right.

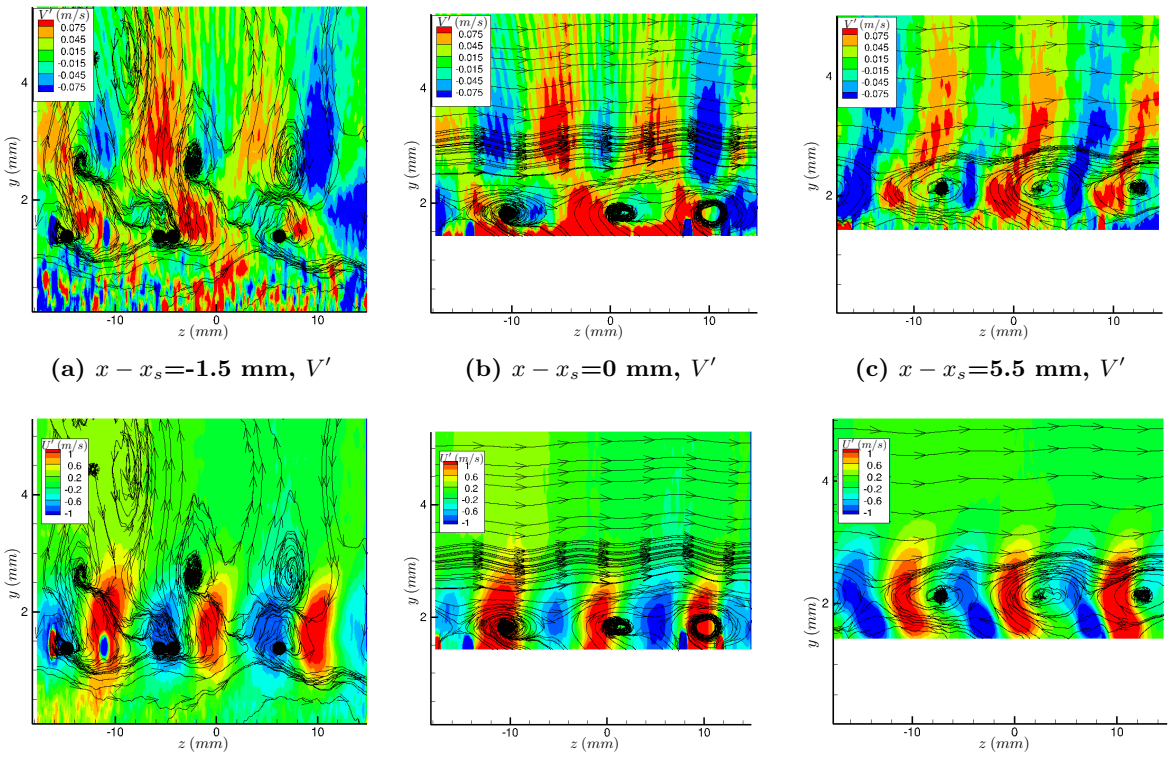

(a) $x - x_s$**=-1.5 mm,** V' **(b)** $x - x_s$**=0 mm,** V' **(c)** $x - x_s$**=5.5 mm,** V'

(d) $x - x_s$**=-1.5 mm,** U' **(e)** $x - x_s$**=0 mm,** U' **(f)** $x - x_s$**=5.5 mm,** U'

Figure 16: Spanwise planes upstream and downstream of the step for the 1.4 mm FFS with four layers of DREs. Colors are U' and V' contours. In-plane streamlines are included as black lines.

The behavior immediately upstream and downstream of the 1.7 mm FFS is very similar to the 1.4 mm step case. The main difference between these two cases is the larger region of crossflow reversal that was measured downstream of the step for the larger step height. Several planes downstream of the step are shown for the 1.7 mm FFS case in Fig. 17 to illustrate the effect of the crossflow reversal region. These figures include color contours of the U' and V' velocity along with the in-plane streamlines. Due to the positive crossflow component that develops near the surface, there are now two inflection points in the $\partial W_{cf}/\partial y$ profiles (as shown in Fig. 10). Thus, two sets of vortices are present, even though there is only one peak in the V'_{rms} profile near the wall. These vortices are rotating in opposite directions, with the upper set rotating clockwise and the lower set rotating counter-clockwise. The lower set of vortices is just starting to become evident at 3 mm downstream of the step (Fig. 17d). As in the 1.4 mm FFS case, the upper set of V' disturbances (at $y \approx 2$ mm) gets lifted up above the influence of the new vortices that develop downstream of the step. In fact, in this case, the amplitude is so small they are hardly visible anymore. Farther downstream, the V' velocity becomes large in amplitude and starts to broaden in the y direction, as is evident in Fig. 17c. There are also harmonics that are starting to become apparent at this location, particularly near the wall.

Looking at the U' contours (Figs. 17d-17f), there are two sets of disturbances present, which agrees with the double-peaked U'_{rms} profiles shown in Fig. 13a. Similar to the 1.4 mm FFS case, the upper set, which is located at approximately y=1 mm, corresponds to the U' disturbance that directly impacted the step, and the amplitude decays downstream since there is no stationary crossflow vortex acting to enhance it. The lower set, located very close to the surface, develops due to the strong vortices that develop near the wall just downstream of the step. As the flow progresses downstream, the upper set of U' disturbances decreases in amplitude and becomes offset in phase from the lower set. This is primarily due to the outboard shift in location of the lower set of U' disturbances. By $x - x_x$=18 mm, the offset is nearly 180°.

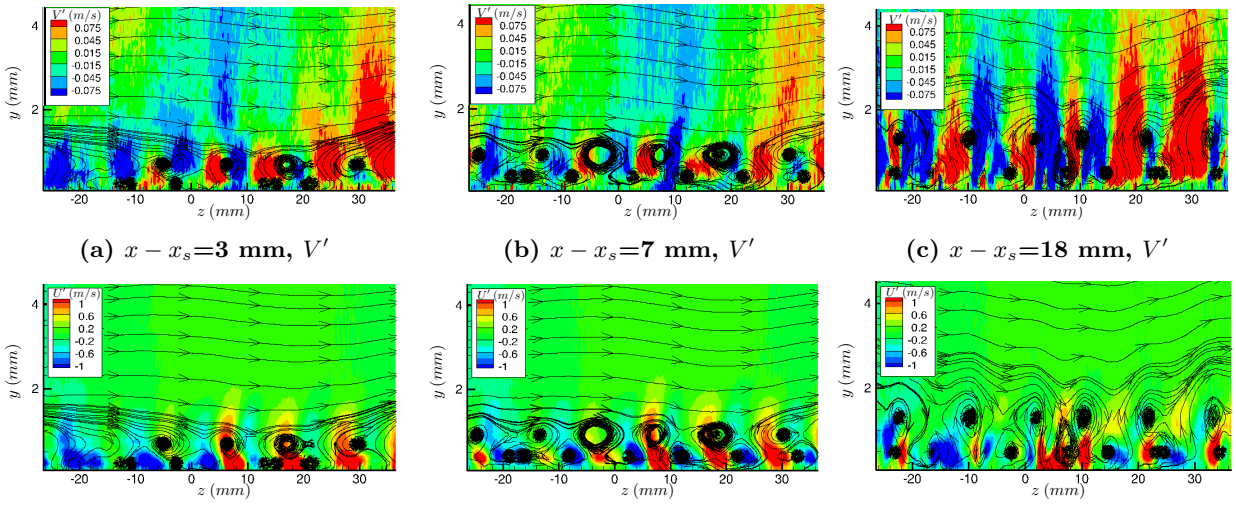

(a) $x - x_s$**=3 mm,** V' **(b)** $x - x_s$**=7 mm,** V' **(c)** $x - x_s$**=18 mm,** V'

(d) $x - x_s$**=3 mm,** U' **(e)** $x - x_s$**=7 mm,** U' **(f)** $x - x_s$**=18 mm,** U'

Figure 17: Spanwise planes showing U' and V' velocity (color contours) along with in-plane streamlines (black lines) for several locations downstream of the 1.7 mm FFS.

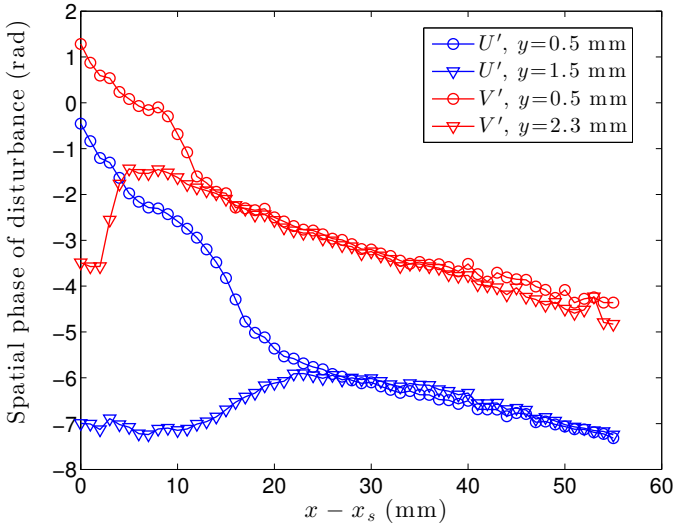

Figure 18: Spatial phase of U' and V' disturbance vs. x for the 1.7 mm FFS case.

This behavior of the lower and upper U' disturbances can be shown more clearly by computing the spatial phase of the U' velocity at each y-location inside the boundary layer and for each streamwise station. This analysis is performed for both the U' and V' velocity, and the phase is computed for the primary 11 mm wavelength. The results are shown in Fig. 18 for the lower and upper disturbances. Since the upper V' disturbance sits a little above the upper U' disturbance, the chosen y locations for the two upper disturbances are different, as noted in the legend. Notice that the initial phases of the U' disturbance (at $x - x_s$=0 mm) are actually more similar than they appear (since 0 and 2π are actually the same angle). However, since the lower set of U' disturbances tends to travel outboard, the phases become offset, and the lower U' disturbance actually travels almost a whole wavelength before it joins up again with the upper disturbance. The two phases align and remain almost identical from shortly downstream of $x - x_s \approx$20 until the end of the last measurement station. Note that this is approximately the location where the U'_{rms} amplitude begins to grow for the second time.

The V' disturbances behave similarly, however, the region where the two disturbances realign occurs approximately 10 mm farther upstream than for the U' disturbances. This location, $x - x_s \approx$ 10 mm,

corresponds to the location where the V'_{rms} profiles begin to suddenly become very broad, as shown in Figs. 12e and 13b. Thus, it appears that the combination of the upper and lower sets of V' disturbances is what leads to this broadening and continued growth of V'_{rms}. It is surprising that the upper V' disturbance appears to still play a role in this scenario since the upper peak practically disappears from the V'_{rms} profile. This type of behavior supports the conjecture mentioned earlier that the second region of growth is due to a nonlinear mechanism.

As usual, the behavior of U' can be explained from the behavior of V'. Remember that where V' is negative, U' should be positive. This implies that the phases of V' and U' should be offset by approximately 180°. Notice that the offset of the U' and V' phases near the wall at $x - x_s$=0 is approximately 1.5 rad, or 90°, not 180°. The reason for this offset was explained earlier. The phases of U' and V' at y=0.5 mm follow each other closely until the point where the upper and lower V' disturbances join. At this point, the U' phase continues to decrease rapidly, until it reaches a point where it is approximately 180° out of phase with V'. This is the point where it joins up with the upper U' phase. Physically, this means that the U' disturbance takes some time to recover and catch up with the action of the vortices, since it is initially offset from V' due to the sudden introduction of the step. Once it catches up and merges with the upper U' disturbance, then the U'_{rms} amplitude growth occurs.

This behavior is further illuminated by examining the U' contours at two different heights above the surface. Planform views of the U-disturbance velocity are shown in Fig. 19 at two different y locations for four of the cases studied. For the 1.7 mm FFS case (Fig. 19a) near the wall and very near the step, the U' contours bend outboard fairly aggressively until straightening out farther downstream. The near-wall streamlines are included on this plot to show that the contours appear to follow the near-wall streamlines close to the step rather than the inviscid streamlines. This is very different from the behavior at y=1 mm (Fig. 19e), in which the contours follow a fairly straight path downstream, much closer to the path of the external streamlines, though they do curve slightly inboard of the streamlines near the step. The 1.52 mm and 1.6 mm FFS cases exhibit this same behavior, though they are not included in this figure. Thus, for the large step heights, the near-wall vortices appear to follow the near-wall streamlines downstream of the step, which causes the migration of the V' and U' contours seen in Fig. 18.

The path taken by the U-disturbance contours for the 1.4 mm FFS case varies somewhat depending on the stationary crossflow amplitude. For the lower amplitude case (Fig. 19b), the contours near the step do curve slightly outboard with the near-wall streamlines, though not nearly as aggressively as for the larger step cases. However, when the stationary crossflow amplitude is increased (Fig. 19c), the contours near the wall actually appear to curve inboard, more closely following the path of the outer (y=1 mm) contours. For the smallest step case, 1.27 mm, the U' contours near the wall curve just slightly outboard for a short region downstream of the step, before straightening out and aligning with the streamlines. The U' contours at y=1 mm essentially follow a similar path, though they also curve slightly inboard of the external streamlines, as in the 1.4 mm FFS case.

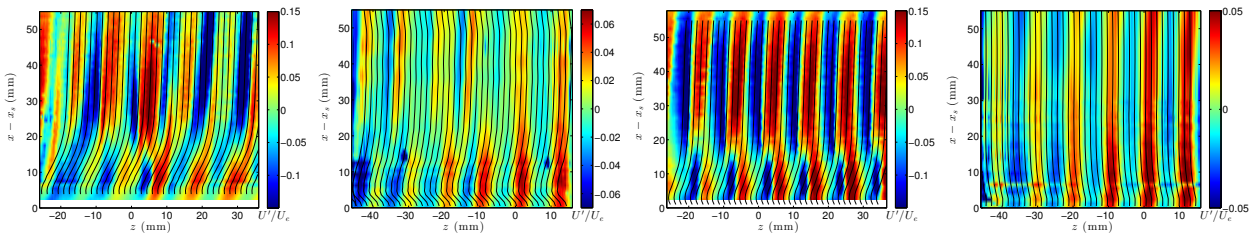

(a) 1.7 mm FFS, y=0.5 mm (b) 1.4 mm FFS, y=0.5 mm (c) 1.4 mm FFS, 4 layers DRES, y=0.5 mm (d) 1.27 mm FFS, y=0.5 mm

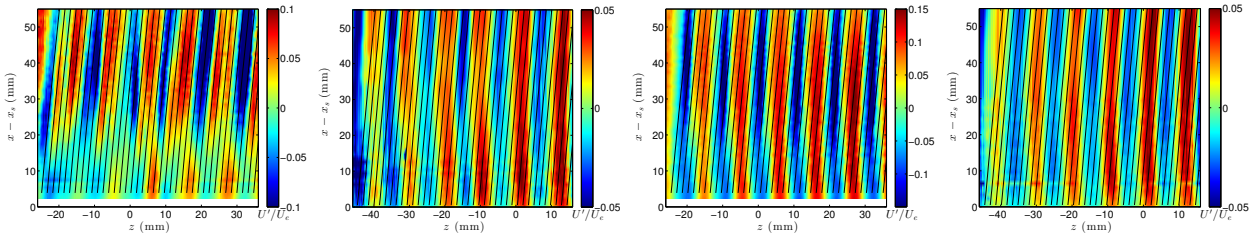

(e) 1.7 mm FFS, y=1 mm (f) 1.4 mm FFS, y=1 mm (g) 1.4 mm FFS, 4 layers DRES, y=1 mm (h) 1.27 mm FFS, y=1 mm

Figure 19: Planform view of U-disturbance velocity at two different wall-normal locations. Black lines are streamline contours. Plots (a)-(d) include near-wall streamlines ($y \approx 0.1$ mm), while plots (e)-(h) include inviscid streamlines.

D. Effect of Steps on Unsteady Disturbances

Another interesting aspect of the flow that was illuminated by the time-resolved PIV is the manner in which breakdown occurs downstream of the step. The u'_{rms} contours at y=0.5 mm are shown in Fig. 20 for the three largest step heights, and for the 1.4 mm FFS case with 4 layers of DREs. The other cases did not exhibit any substantial u'_{rms} growth, so they are not included in this figure. For the 1.52 mm FFS height (Fig. 20c), a u'_{rms} disturbance begins to appear toward the inboard side of the measurement area starting at approximately 25 mm downstream of the step. The u'_{rms} disturbance appears progressively closer to the step as the step height is increased, and the amplitudes reach larger values. For the 1.4 mm FFS case with four layers of DREs (Fig. 20d), the u'_{rms} disturbance is apparent immediately downstream of the step. It appears to decays for a short distance before it grows again significantly at 15 mm downstream of the step. Given the local nature of this disturbance, and the fact that it appears for the 1.4 mm FFS case with larger amplitude stationary crossflow but not for the same step height with lower amplitude stationary crossflow, this is likely a secondary instability of some type. However, it is interesting that for most cases the instability begins to appear at the x-location where the amplitude of the stationary crossflow is at a minimum.

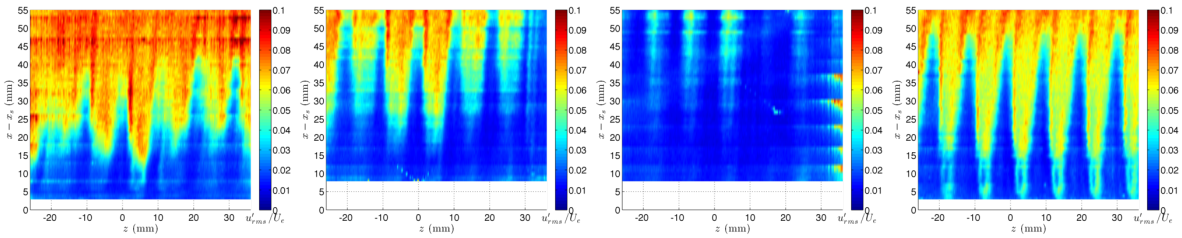

(a) 1.7 mm FFS (b) 1.6 mm FFS (c) 1.5 mm FFS (d) 1.4 mm FFS, 4 layers DRES

Figure 20: Planform view of u_{rms} velocity at y=0.5 mm for four step heights.

Time-resolved PIV results were acquired at 8 kHz for several select conditions and locations to try to learn more about the nature of these instabilities. The TRPIV results revealed a high-frequency instability

beginning shortly downstream of the step for the critical step heights. The peak frequency occurs between 0.5 to 2 kHz, depending on the step height and location as shown in Fig. 21. This figure shows the spanwise-averaged spectra at various streamwise locations for the 1.52 through 1.7 mm step heights. This frequency range is approximately that of the high-frequency secondary instabilities seen in the baseline case,[12] which are typical of stationary crossflow breakdown. However, in this case, when these instabilities start to occur, the mean flow (see line contours of Fig. 22) does not resemble the highly inflectional modulated flow that is typically seen when the secondary instabilities begin to be destabilized (such as that seen by White[13] or Malik[14]). In general, the areas of largest amplitude do seem to correlate with areas of large wall-normal shear of the U-velocity ($\partial U/\partial y$), so these high-frequency fluctuations may be associated with a Y-mode type of secondary instability. However, as shown in Fig. 9, $\partial U/\partial y$ is at a maximum near the step, and then decreases downstream. So the area where these unsteady disturbances appear (for 1.52 mm and up) does not correlate with the streamwise region of largest wall-normal shear. Thus, it is unclear what initiates the growth of these disturbances.

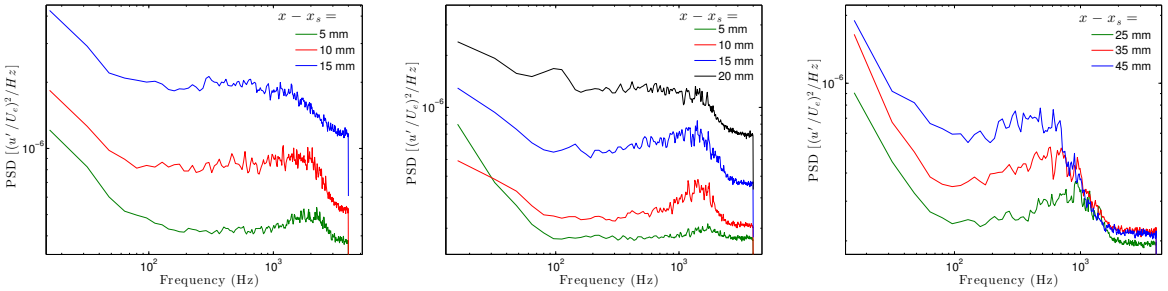

(a) 1.7 mm FFS **(b) 1.6 mm FFS** **(c) 1.52 mm FFS**

Figure 21: Velocity spectra acquired at y=0.6 mm for several streamwise location and three different step heights.

Proper orthogonal decomposition (POD) was used to gain more information about these high-frequency instabilities. The data were first band-pass filtered between 500 to 2700 Hz to isolate the frequency range of interest. Then, POD was performed on all 10,000 images to acquire the most energetic mode. This mode is plotted in Fig. 22, along with the mean flow contours (lines) for three different step heights and locations. These locations were chosen for each step height to be shortly downstream of where the disturbance becomes noticeable in Fig. 20. The width of the image had to be cut down to obtain the higher acquisition rate, so the spanwise extent of these high-speed measurements was only slightly larger than one wavelength of the primary stationary crossflow mode. As expected, the disturbances occur locally, with a spanwise spacing similar to the stationary crossflow mode spacing (11 mm). It is interesting to note that for the two smaller step height cases shown here, the two disturbances that were captured appear to be in phase, while for the 1.7 mm step case, they appear to be approximately 180° out of phase.

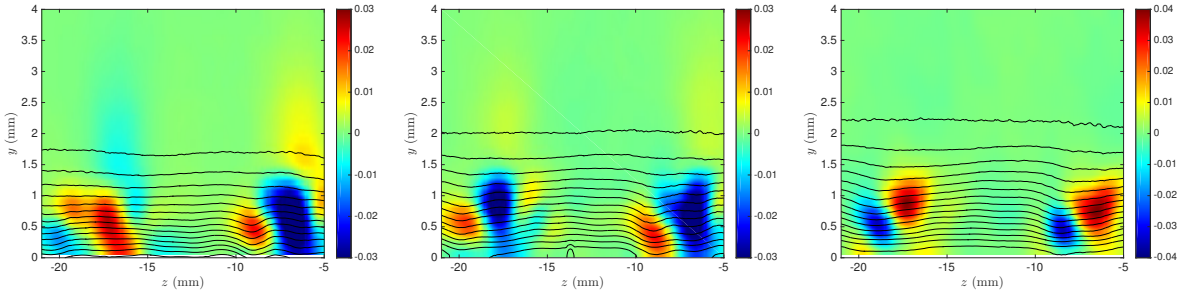

(a) 1.7 mm FFS, $x-x_s$=10 mm **(b) 1.6 mm FFS, $x-x_s$=20 mm** **(c) 1.5 mm FFS, $x-x_s$=35 mm**

Figure 22: First POD modes for three different step heights.

IV. Conclusions

The transition process on a swept wing over a forward-facing step is a highly complex process. Most of the step heights studied resulted in a strong region of growth of U'_{rms} just downstream of the step, followed by a short period of decay, and a second region of growth. The amplitudes and lengths of these periods of growth and decay varied with step height. There is not a very clear dividing line between the critical and subcritical step heights. The two largest step heights (1.6 mm and 1.7 mm) resulted in upstream movement of the transition front, as did the 1.4 mm FFS case with increased stationary crossflow amplitude. The 1.52 mm step resulted in significant growth of the stationary crossflow downstream of the step, but the amplitude eventually returned to that of the baseline case and premature transition was not observed. The 1.4 mm FFS resulted in a small amount of growth just downstream of the step, and it also resulted in a second region of growth, similar to the larger step cases, but the amplitude and growth rate were much smaller. The smallest step height studied, 1.27 mm, resulted in only a small increase in amplitude downstream of the step, but no significant second region of growth.

It is clear that the stationary crossflow instabilities are strongly influenced by the step, but the challenge is determining the underlying mechanism. Upstream of the step, the primary incoming stationary crossflow vortices are lifted up by a significant amount, so they do not directly impact the step. However, there appears to be another set of vortices that form underneath the primary set. These vortices are rotating in the opposite direction due to the crossflow reversal that occurs near the wall. It is this secondary set of vortices that directly impacts the step. Since they are rotating in the opposite direction, they should not interact constructively with the helical flow region downstream of the step. They could interact constructively if they impacted the step below the center of the vortex, but this does not appear to be the case.

Immediately downstream of the step, the location of the inflection point in the crossflow profile shifts closer to the surface. The V' disturbances created by the lower incoming stationary crossflow vortices become important downstream of the step because they persist close to the surface, right at the new location of the inflection point. This means that the vortex that is caused by the strong negative crossflow region right at the step can feed off this V' disturbance. In addition, the wall-normal gradient of the streamwise velocity, $\partial U/\partial y$, is very strong near the step and decreases downstream, which follows the growth and decay pattern of U'_{rms}. Thus, it is believed that the combined effects of the incoming V' amplitude near the step, the strong negative crossflow region at the step, and the behavior of $\partial U/\partial y$ result in the initial growth and decay of U'_{rms} starting at the step. It is interesting to note that the growth rates of U'_{rms} and V'_{rms} are very similar for both of the 1.4 mm FFS cases throughout this region even though the stationary crossflow amplitudes are very different. This would indicate that the growth in this region is linear, which would be expected if it is primarily an effect of the mean flow distortion due to the step. This initial short region of crossflow growth does not appear to directly lead to transition for any of these cases. Rather, it is downstream of the second region of growth where transition occurs.

The second region of growth of the U'_{rms} amplitude appears to be related to the merging of the upper and lower V' disturbances, which leads to the merging of the upper and lower U' disturbances. The upper and lower sets of V' disturbances are initially offset coming into the step due to the development of the two sets of vortices upstream of the step. Downstream of the step, the lower V' disturbances travel strongly outboard with the streamlines near the wall, until they merge with the upper set of disturbances. It was demonstrated that two vortices exist downstream of the larger steps due to the crossflow reversal region that occurs, which causes two inflection points in the crossflow profile. This crossflow reversal region occurs near the wall just downstream of the brief negative crossflow region, and the strength and size of this region increases with increasing step height. The near-wall V' disturbances grow throughout this process due to these two sets of vortices. Once they join up with the upper set of V' disturbances, which still exist though they have decayed significantly from upstream, the V'_{rms} profiles broaden significantly, and the amplitude continues to grow. It is believed that this region of growth is nonlinear. The growth does not appear to be related to anything that is happening in the mean flow, and it is shown that increasing the stationary crossflow amplitude (i.e., for the 1.4 mm FFS case) results in a significant increase in the growth rate of V'_{rms} and U'_{rms} during this region.

As mentioned, it is during this downstream region of growth that transition is triggered. The crossflow reversal region downstream of the step occurred for the step heights that caused increased growth of the stationary crossflow (even if transition was not triggered earlier), with increasing severity as the step height was increased. It is believed that this crossflow reversal region plays a crucial role in the transition process downstream of the step for two reasons. The first is the effect of the near-wall vortex, which is caused by

the crossflow reversal, on the growth of the near-wall V' disturbance. The second is the strong outboard streamline curvature near the wall that exists due to the positive crossflow component. It is this strong streamline curvature that causes the upper and lower sets of V' disturbances, which initially start out offset by approximately 180°, to merge downstream, leading to the strong downstream growth of the stationary crossflow. Thus, the existence of a crossflow reversal region downstream of the step may be a good indicator of whether a case will be critical or not. It remains to be seen whether this holds true for other geometries and flow conditions.

It was also demonstrated that increasing the incoming stationary crossflow amplitude can cause a previously subcritical step height to become critical. This particular step height (1.4 mm) may have been right on the edge of being a critical step height. It did exhibit similar behavior to the two critical step heights studied. In particular, the stationary crossflow amplitude followed a similar growth and decay pattern to the larger step heights. However, there were also some interesting differences between the 1.4 mm FFS case with 4 layers of DREs, which led to early transition, and the two critical step heights of 1.6 mm and 1.7 mm. The upper peak in the U'_{rms} amplitude decayed significantly more for the two larger step heights than for the 1.4 mm case. Additionally, the paths that the near-wall vortices took downstream of the step were different for the 1.4 mm step compared to the larger step heights. Thus, it is not clear whether the mechanisms affecting the growth of the stationary crossflow for this case are exactly the same as the larger step cases. This does show that it is important to consider the effect of stationary crossflow amplitude when attempting to predict a critical step height.

A limited amount of unsteady measurements were presented as well. The growth of the unsteady disturbances begins near the region of second growth of the U'_{rms} amplitude. The fluctuations correspond to a high frequency disturbance with frequencies similar to the high-frequency secondary instabilities measured in the baseline case. The locations of the peak fluctuations appear to correspond roughly to regions of high wall-normal shear of U ($\partial U/\partial y$) in the spanwise planes. However, they do not occur farther upstream where $\partial U/\partial y$ is at its maximum, and where U'_{rms} is very large. More research is required to determine the primary source of these disturbances.

References

[1]Malik, M. R., Crouch, J. D., Saric, W. S., Lin, J. C., and Whalen, E. A., "Application of Drag Reduction Techniques to Transport Aircraft," *Encyclopedia of Aerospace Engineering*, 2016.

[2]Crouch, J., Kosorygin, V., and Ng, L., "Modeling the effects of steps on boundary-layer transition," *IUTAM Symposium on Laminar-Turbulent Transition*, Springer, 2006, pp. 37–44.

[3]Wörner, A., Rist, U., and Wagner, S., "Influence of humps and steps on the stability characteristics of a 2D laminar boundary layer," AIAA Paper 2002-0139, 2002.

[4]Drake, A., Bender, A., Korntheuer, A., Westphal, R., McKeon, B., Gerashchenko, S., Rohe, W., and Dale, G., "Step Excrescence Effects for Manufacturing Tolerances on Laminar Flow Wings," AIAA Paper 2010-375, 2010.

[5]Perraud, J. and Seraudie, A., "Effects of Steps and Gaps on 2D and 3D Transition," *European Congress on Comp. Methods in Applied Science and Eng., ECCOMAS*, 2000, pp. 11–14.

[6]Duncan Jr, G., Crawford, B., and Saric, W., "Effects of Step Excrescences on Swept-Wing Transition," AIAA Paper 2013-2412, 2013.

[7]Duncan Jr, G. T., Crawford, B. K., Tufts, M. W., Saric, W. S., and Reed, H. L., "Effects of Step Excrescences on a Swept Wing in a Low-Disturbance Wind Tunnel," AIAA Paper 2014-0910, 2014.

[8]Tufts, M. W., Reed, H. L., Crawford, B. K., Duncan Jr, G. T., and Saric, W. S., "Computational Investigation of Step Excrescence Sensitivity in a Swept-Wing Boundary Layer," *Journal of Aircraft*, Vol. 54, No. 2, March-April 2017, pp. 602–626.

[9]Eppink, J. L., "Stereo Particle Image Velocimetry Measurements of Transition Downstream of a Foward-Facing Step in a Swept-Wing Boundary Layer," AIAA Paper 2017-0306, 2017.

[10]Saric, W. S. and Reshotko, E., "Review of Flow Quality Issues in Wind Tunnel Testing," AIAA Paper 1998-2613, 1998.

[11]Eppink, J. L., Wlezien, R. W., King, R. A., and Choudhari, M., "Interaction of a Backward-Facing Step and Crossflow Instabilities in Boundary-Layer Transition." *AIAA Journal*, 2017.

[12]Eppink, J., *The Interaction of Crossflow Instabilities and a Backward-Facing Step in Swept Boundary Layer Transition*, Ph.D. thesis, Tufts University, 2014.

[13]White, E. and Saric, W., "Secondary Instability of Crossflow Vortices," *Journal of Fluid Mechanics*, Vol. 525, No. 1, 2005, pp. 275–308.

[14]Malik, M. R., Li, F., Choudhari, M. M., and Chang, C.-L., "Secondary Instability of Crossflow Vortices and Swept-Wing Boundary-Layer Transition," *Journal of Fluid Mechanics*, Vol. 399, 1999, pp. 85–115.